Train–Network Interactions and Stability Evaluation in High-Speed Railways–Part I: Phenomena and Modeling

Haitao Hu, *Member, IEEE*, Haidong Tao, *Student Member, IEEE*, Frede Blaabjerg, *Fellow, IEEE*, Xiongfei Wang, *Senior Member, IEEE*, Zhengyou He, *Senior Member, IEEE*, and Shibin Gao

***Abstract*—This paper presents an impedance-based model to systematically investigate the interaction performance of multiple trains and traction network interaction system, aiming to evaluate the serious phenomena, including low-frequency oscillation (LFO), harmonic resonance, and harmonic instability. The train–network interaction mechanism is therefore studied, and one presents a detailed coupling model for investigating the three interactive phenomena and their characteristics, influential factors, analysis methods, and possible mitigation schemes. In Part I of the two-part paper, the measured waveforms of such three phenomena are first characterized to indicate their features and principles. A unified framework of the train–traction network system for investigating the three problems is then presented. In order to reveal the interaction mechanism, all-frequency impedance behaviors of the electric trains and traction network are equally modeled. In which, an impedance-based input behavior of the train is fully investigated with considering available controllers and their parameters in *DQ*-domain. The entire traction network, including traction transformer, catenary, supply lines, is represented in a frequency-domain nodal matrix. Furthermore, the impedance–frequency responses of both electric train and traction network are measured and validated through frequency scan method. Finally, a generalized train–network simulation and experimental system are conducted for verifying the theoretical results of the two-part paper.**

***Index Terms*—Harmonic instability, harmonic resonance, high-speed railway (HSR), low-frequency oscillation (LFO), train–network interactions.**

Manuscript received October 18, 2017; accepted December 1, 2017. Date of publication December 11, 2017; date of current version February 22, 2018. Recommended for publication by Associate Editor T. M. Lebey. This work was supported by the National Natural Science Foundation of China under Grant NSFC 51677154 and Grant NSFC 51525702. *(Corresponding author: Zhengyou He.)*

H. Hu, H. Tao, Z. He, and S. Gao are with the School of Electrical Engineering, Southwest Jiaotong University, Chengdu 610031, China (e-mail: hht@swjtu.edu.cn; thdswjtu@163.com; hezy@swjtu.edu.cn; gao_shi_bin@126.com).

F. Blaabjerg and X. Wang are with the Department of Energy Technology Aalborg University, Aalborg 9220, Denmark (e-mail: fbl@et.aau.dk; xwa@et.aau.dk).

This paper has supplementary downloadable material available at http://ieeexplore.ieee.org. This includes a video that demonstrates the experimental processes of low frequency oscillations and harmonic stability. This material is 41.4 MB in size.

Color versions of one or more of the figures in this paper are available online at http://ieeexplore.ieee.org.

Digital Object Identifier 10.1109/TPEL.2017.2781880

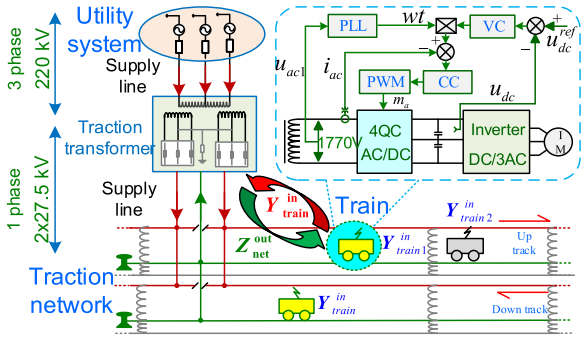

Fig. 1. Typical HSR train–network interaction system.

I. Introduction

With the fast development of worldwide high-speed railway (HSR) along with the widely adoption of the ac–dc–ac voltage source converter (VSC) based high-speed trains (HSTs), the harmonic and interaction instability problems have been frequently appeared and reported in previous literatures [1]–[3]. Among the reported problems, harmonic resonance, low-frequency oscillation (LFO), and harmonic instability have been given more attentions due to the dynamic interactions between multiple trains and traction network, and serious impacts on system power quality and stability. Their adverse impacts not only deteriorate the supply environment of the traction network, but also affect the onboard traction drive, auxiliary and their control systems.

As the train is a typical harmonic and disturbance source operating in the traction network, the large power demand and disturbance will degrade the voltage or power quality of the traction network, which can further deteriorate the stability and safety of the traction drive system. Obviously, as shown in Fig. 1, the train and traction network essentially interact with each other. Three-phase 220 kV power source is stepped down to feed the catenary system through the traction transformer in a traction substation. The traction network not only supplies the energy to the running electric trains but also absorbs the injected harmonics and regenerated power from the trains. Due to different control modes, numbers, positions, and loading conditions of multiple electric trains, the train subsystem of the interaction system show different behaviors interacting with the traction network.

Seen from the traction network side, the electric trains running on the rails are usually represented by a constant current or PQ model for harmonic and power flow studies [8], [9]. Published works have shown that the input admittance of the four-quadrant converters (4QCs) of the HST will affect the traction network analysis, thereby arising the oscillation or instability problem [10]. While seen from the electric train side, the traction network is usually assumed to be a linear multiport impedance-based network. However, the traction network may have inherent impedance behavior or resonance points. Almost all power quality problems in the HSR are caused by the different features of the scheduled trains as well as the traction network.

The standard EN50388-2012 [4], added some new phenomena from its previous version in 2005, described and classified the root causes of the overvoltage problems happening in the ac or dc electrified railways as oscillation (or instability) and harmonic problems. Based on previous literatures, the LFO, harmonic resonance, and harmonic instability phenomena in electric railway systems can be overviewed as follows:

1) *LFO:* from 1 Hz to several hertz, often happens in a rail deport in transformer-based electric railways when multiple trains are simultaneously energizing or operating [5]. Alternatively, the oscillation can also be caused by the rotatory frequency converter in some European railway systems, such as Norway, Sweden [6]. Consequently, the oscillatory voltage and current waveforms contain a significant low-frequency component.
2) *Harmonic resonance:* often from a few hundred to kilohertz, has been widely reported in many HSR systems due to the interaction between capacitive and inductive network parameters. As a distributed *RLC* circuit, the catenary network can experience series or parallel resonances at one or multiple specific frequencies that amplifies the harmonic currents generated from electric trains and leads to the interference in adjacent communication lines and the rail signaling system, overheating, and vibration at the power capacitors, and mal-operation at the protections [2], [3].
3) *Harmonic instability:* typically a few hundred hertz, is caused by the feedback loop of network-connected 4QCs of electric trains, was first reported in Zürich (Switzerland) in 1995 [1] where the electric train emits excessive harmonic currents due to instability. As the instability originate from destabilization of poorly damped harmonic resonances, this phenomenon is also known as resonance instability or harmonic instability [7]. The harmonic instability may lead to continuous amplification of voltage waveforms with a high-harmonic content and lead to the significant harmonic overvoltage either at the train location or in other positions along the traction network.

Therefore, in order to investigate the characteristics of the three phenomena in a unified framework, the input or output equivalent "admittance" or "disturbance" in train–network interaction system should be fully considered. There are many published documents focusing on the modeling and analysis of the electrical characteristics in electric railway systems [2], [3], [11]–[15]. However, they simplified the model of either the electric train system or the traction network for harmonic or stability problems and studied the three phenomena separately. Thus, this paper and the companion one are organized to investigate these problems.

TABLE I
LOW-FREQUENCY OSCILLATION CASES WITH A ROTARY CONVERTER

No.	f_1 (Hz)	f_0 (Hz)	Time	Located
1	1.6	16.67	2007	Norway [6]
2	1.2	25	1997	America [16]
3	1.6	16.67	1991	Germany [17]
4	1.9	16.67	1991	Germany [17]

In this two-part paper, we aim to investigate and improve the electrical interaction performance between the traction network and multiple electric trains. Part I of the two-part paper systematically characterizes the phenomena of the harmonic resonance, LFO, and harmonic instability, focusing on phenomena description and impedance modeling of the train–network system. The field tests in electric railway systems are organized in order to reveal the train–network interaction mechanism or laws. Part II of the paper will present detailed simulations and experimental results to assess and validate the influential factors, relationship among the three phenomena in a unified impedance-based framework.

II. FIELD PROBLEMS IN HSR

In order to investigate the electrical characteristics of the three different phenomena (i.e., LFO, harmonic resonance, and harmonic instability), various associate field data have been presented and discussed in this section.

A. Field Tests of the LFO

There are two types of LFO scenarios dependent on the rotary frequency converter existing or not. Some electrified railways in Norway, America, Sweden, Germany, and Switzerland have adopted the rotary frequency converter as the power supply solution [6], [16], [17]. The LFO has been early reported from those railway systems. Table I surveys the LFO cases which adopted a rotary converter in electric railway systems over the world [18]. The typical oscillatory frequency $f_{\rm osc}$ $(f_0 - f)$ is approximately $10\%-30\%$ of the respective power system's fundamental frequency f_0. The rotary converter, used for the power supply mode variations in traction substation, is exciting oscillations, i.e., given by active power changes in the 16⅔-Hz ac railway system. The oscillation is critical stable and the damping of the system is insufficient even negative.

The second scenario of LFO phenomena mainly happened in a rail depot, where multiple trains are prepared for operating and located far from the traction substation. Multiple trains in the rail depot have rose the pantographs to energize, leading to a 0.6–7 Hz LFO of the catenary voltage. As a result, the 4QCs of electric trains were therefore locked and shut down by protection devices due to the transient fluctuated overvoltage. Alternatively, different types of electric trains in different railway systems have experienced similar LFOs in other rail depots, and the oscillatory frequencies were not the same. Some cases of the

TABLE II
LFO CASES WITHOUT A ROTARY CONVERTER [19]

No.	f_1 (Hz)	f_0 (Hz)	time	Case
1	5	50	2008	Thionville, France [20]
2	7	50	2006	Siemens test, Germany [21]
3	3	25	2006	Washington, DC, USA [22]
4	5	16.67	1995	Zurich, Switzerland [23]
5	2–4	50	2008-01	Hudong Depot, HX_D 1
6	5	50	2010-01	Shanghai Nanxiang, CRH_1
7	5	50	2010-09	Qingdao Depot, CRH_5
8	0.6–2	50	2015-12	Xuzhou Hub, HX_D 2B
9	6–7	50	2011-11	Shanhaiguan Hub, HX_D 3B

Note: The default location of the listed cases is in China.

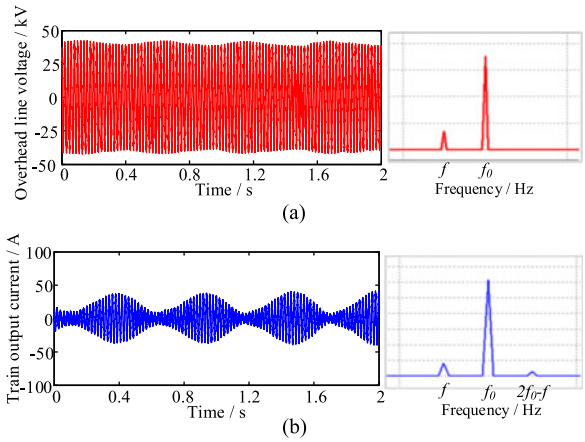

Fig. 2. Measured waveforms of LFO: (a) voltage waveform and its spectrum; (b) current waveform and its spectrum.

LFO phenomena happened in a rail depot without the rotary converter are listed in Table II.

Fig. 2 shows the measured waveforms under LFO condition in Xuzhou hub substation of Jiangsu Province, China. It represents a typical measured voltage and current waveforms under an LFO. The harmonic spectrum of the current waveform absorbed by the electric train is composed of two interharmonic components, which are symmetrically superimposed to the fundamental frequency f_0, and corresponds to the frequency of the voltage excitation into consideration.

Fig. 3 depicts the measured waveforms of LFO in Cangkou traction substation of Shandong Province, China. The measurements of the LFO in a railway deport with the increasing number of electric trains connected to the traction network are shown in Fig. 3, where the voltage and current waveforms are oscillating when the sixth train is connecting. Moreover, the oscillatory frequencies in Fig. 3(b) and (c) are different as the result of one more train connected. It is worthy noted that the traction lockout (which means that the main circuit breaker of the train trips, the network current is going to be zero, and the dc-link voltage is also decreased) aroused in the tested train, owing to the voltage and current fluctuated intensely at the period of 350–500 ms. It indicates that more electric trains may easily destabilize the traction network and change the oscillatory frequency.

Furthermore, in order to illustrate different oscillatory frequencies and modes, field tests have been taken in Xuzhou railway deport in China in January 2016. When seven or eight

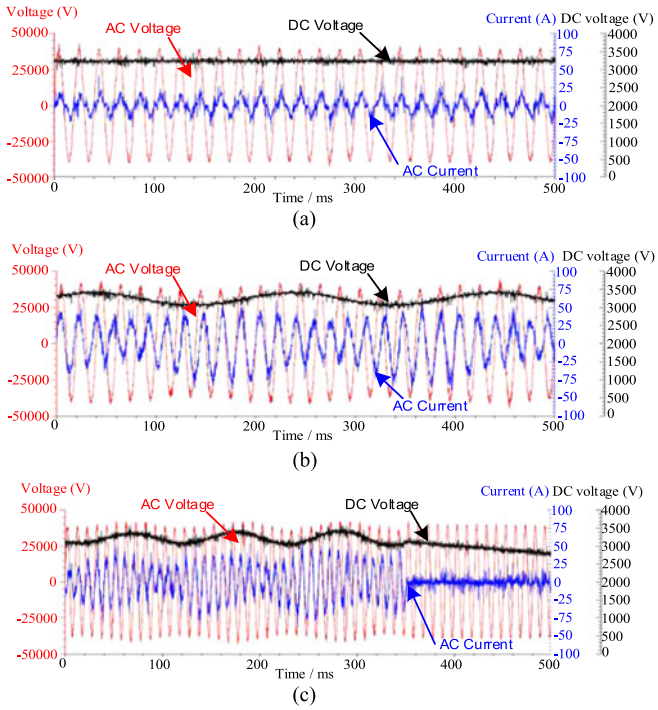

Fig. 3. Measured voltage and current waveforms with different train numbers: (a) less than five trains; (b) six trains; (c) seven trains.

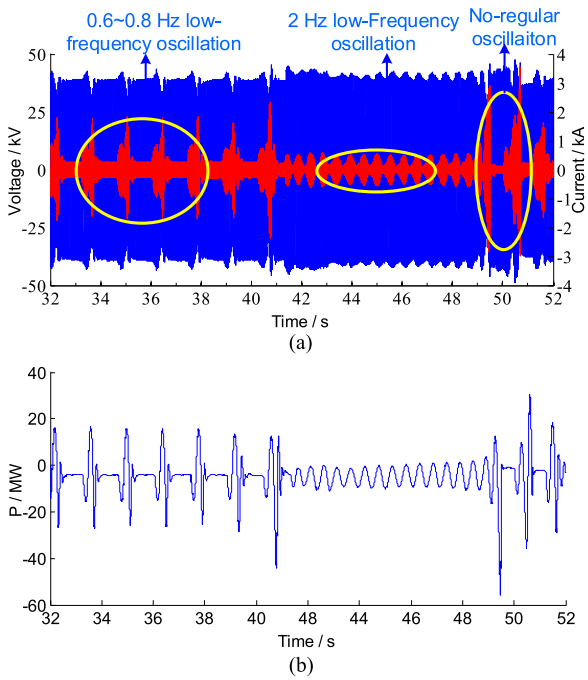

Fig. 4. Measured data of different oscillatory modes: (a) the test waveform of voltage and current; (b) the test oscillation of the active power.

trains connected to the traction network, the voltage and current waveforms of the traction network started to oscillate. Meanwhile, the oscillatory voltage and current waveforms measured in the train are shown in Fig. 4.

Obviously, they may have three different oscillatory modes involved: 1) periodical fluctuation around 0.6 to 0.8 Hz and the oscillation is in critical unstable mode; 2) periodical fluctuation

TABLE III
HARMONIC RESONANCE FIELD CASES IN TPSS

No.	Frequency (pu)	Time	Location
1	17–18	2008-05	Hewu HSR, China [11]
2	50–55	2011-01	Jinghu HSR, China [24]
3	50–55	2010	Boao HSR, China
4	20–25	2004	Shinchungju–Yongjung and Pyongtaek–Maha HSR, Korea [2]
5	39	2011	Italy [14]
6	17–21	2006	Britain [25]
7	3–7	2009	Unknown, Spain [26]

around 2 Hz and the oscillation is highly damped; and 3) irregular fluctuation and the oscillation is getting unstable. Among them, irregular fluctuation contributes to the worst current amplification (about 4000 A). The three oscillatory modes and their oscillatory amplitudes can be found in Fig. 4(b). Experiences from China railway system show that the critical number of trains leading to an LFO is about 6–8, depending on the grid strength and train types. It should be mentioned that the short-circuit capacity of the utility system is usually below 500 MVA and is usually regarded as a weak grid. An LFO happens easily under the condition of a weak supply network and a large number of the electric trains.

B. Field Problems of Harmonic Resonance

The current harmonics generated from a modern train may be amplified by the network harmonic resonance at some specific frequencies in the traction network [13], [15]. The harmonic resonance is an inner nature of an industrial power system and may cause some serious power quality problems like voltage/current distortion, overvoltage with capacitive devices, and interference problems with secondary measurement system and electromagnetic interference with the communication system [14], [15]. The resonance phenomena, which are surveyed in Table III, have been widely reported around the world.

The harmonic resonance phenomenon has been frequently happening in many electric railway systems, and the parallel resonant frequency ranges from 11 to 55 pu with the different traction network topologies and corresponding parameters, which are listed in Table III. On the other hand, Sainz *et al*. [26] reported the series resonance phenomenon considering the connection of the Steinmetz circuit, and the series resonance frequency is about 3–7 pu. In this paper, we mainly focus on the parallel resonances due to the amplification of voltage distortion and their severe adverse impacts on system operations. Figs. 5–7 show some measured field waveforms under harmonic resonance conditions in China HSR system. Those phenomena have been tested in the same or similar supply conditions, and they can be illustrated by the following principles:

1) A serious harmonic distortion occurs on JingHu HSR, as shown in Fig. 5; where Fig. 5(a) shows the voltage and current waveforms of the train and Fig. 5(b) illustrates the corresponding current spectrum of Fig. 5(a). It can be found obviously from Fig. 5(b) that the resonance appears

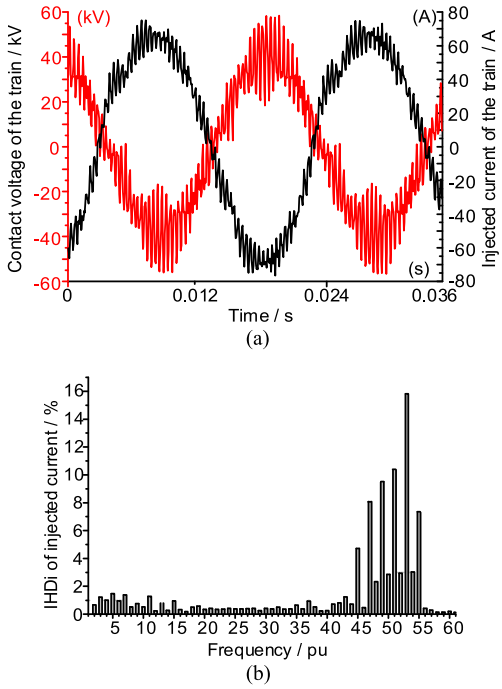

Fig. 5. Harmonic distortions in the leading segment of JingHu HSR: (a) voltage and current waveforms of the CRH380AL electric train; (b) the individual current distortion of measured current.

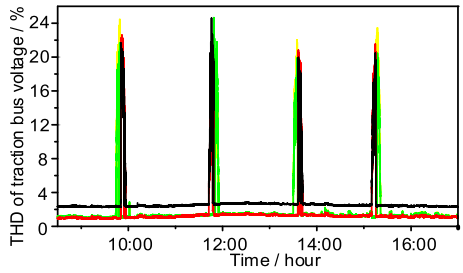

Fig. 6. Total harmonic distortion of traction bus voltage in Qionghai section post, Haidong Line of China.

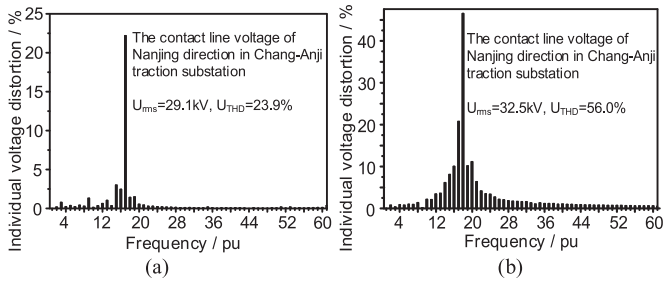

Fig. 7. Harmonic distortions in Changanji TSS, HeWu HSR: (a) time 12:20, resonance frequency is 17 pu; (b) time 14:19, resonance frequency is 18 pu.

in the two times of the switching frequency of the train (for CRH380AL, the switching frequency is 1250 Hz). In Fig. 6, the harmonic resonance occurs periodically in the Qionghai section post, and this periodicity is closely related to the operation interval and the schedule of the rolling stock. The measurements show that the harmonic

TABLE IV
HARMONIC INSTABILITY IN POWER SYSTEMS AND TPSS

No.	Items	Time	Location
1	Railway	1995	Zürich, Switzerland [1]
2	HVDC	1965	Kingsnorth, England [27]
3	Wind generation	2012	Denmark, Poland [28]
4	Solar panel	2004	Amersfoort, Netherlands [29]
5	Railway	2015	Chengdu, China

resonance phenomenon in electric railway systems is generated by the traction network along with fixed positions of substations and the flexible positions and the numbers of the trains. Their parameters matched specific operation conditions.

2) The same conditions of the traction network may excite multiple different frequencies of the harmonic resonance, as shown in Fig. 7. It illustrates that the harmonic resonance corresponds to the electric parameters of the electric train. In other words, the electric train is not only the excitation source of harmonic resonances but also the participative network component. Different positions, powers, and numbers of the trains may change the system impedance and the associated resonance frequencies.
3) From Figs. 5 to 7, the harmonic resonance varies with different traction networks and rolling stocks (e.g., train types, organization, and schedule). Many influential factors might affect the harmonic resonance, such as the parameters of catenary network and traction transformer. Then the essence of harmonic resonance is caused by the traction network matched with the train parameters.

C. Field Problems of Harmonic Instability

The harmonic instability phenomenon in the electric railway was first reported in Zürich, Switzerland, in 1995 [1], due to the adoption of new type trains, which used high-frequency pulsewidth-modulated (PWM) converters, and this phenomenon was then defined in EN50388-2012 [4]. The PWM converter injects massive harmonic currents and shows a negative damping to the traction network. This phenomenon has also been frequently reported in high-voltage direct current systems (HVDC) and VSC-based renewable energy interactions. The typical scenarios of the harmonic or harmonic instability problems in the power system and electric railway system are listed in Table IV.

Fig. 8 presents the measured unstable voltage waveforms of the harmonic instability in Rongchang traction substation of Chongqing, China. The harmonic components are sustained amplified. There is one or multiple resonance points resulting from the interaction between the traction system and a long power cable. However, the harmonic resonance is a stable harmonic amplification in a passive network. In contrast, the unstable harmonic distortion involves active devices with faster controllers, such as the PWM converter of HSTs. These converters can easily become unstable under a network-side resonance situation with a poorly damped network. The controllers [e.g., current controller, voltage controller, and phase-locked loop (PLL)] of the 4QC interact with the passive components in the traction network, leading to harmonic instability problems [29], [30].

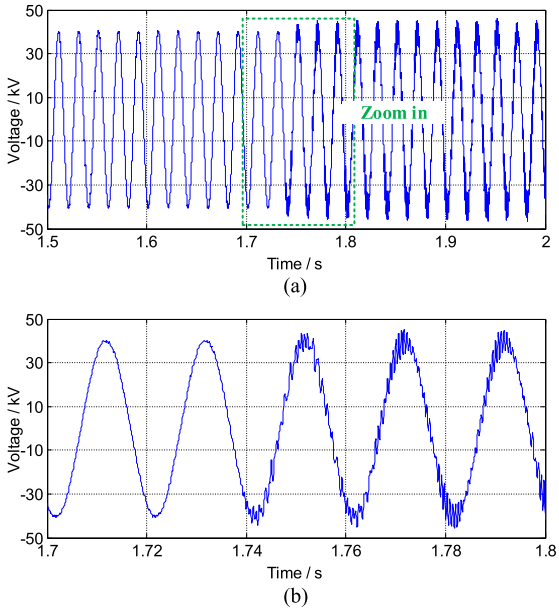

Fig. 8. Measured supply voltage of HST under harmonic instability: (a) voltage waveform of the traction substation; (b) zoom-in view of the turning point.

D. Summary

The mentioned phenomena might deteriorate and destabilize both the traction network and the utility grid. Moreover, the electric trains would easily be shut down by the protective equipment because of the LFO, harmonic resonance, or harmonic instability. An overview of the typical oscillatory waveforms, the matched operating conditions, and their characteristics for the three phenomena are summarized in Fig. 9. Meanwhile, the potential influential factors in terms of the train–network interaction system are involved in the analytical models in an impedance-based framework.

On the basis of the discussions in this section, the three interactive phenomena can be preliminarily summarized as follows.

1) LFO: happens usually under the weak supply system and a number of trains condition from our field test. The simultaneously energization of multiple trains cause the voltage fluctuations and lead to an LFO. The oscillation is mainly dependent on the equivalent impedance ratio between the traction network (corresponding to the supply distance and system capacity) and the train system (corresponding to the connection number of the trains and their control parameters).

Generally, it is assumed that the voltage oscillation is a critical condition of the normal operation. Most of the time, the trains are disconnected the power supply by the software protection, which detects an outage of fluctuated pantograph voltage or a false pantograph bouncing. Moreover, due to the power fluctuation, the upstream power system may cause flicker effect, which forces the power plant to disconnect the railway substation as well as causes a shutdown of the traffic.

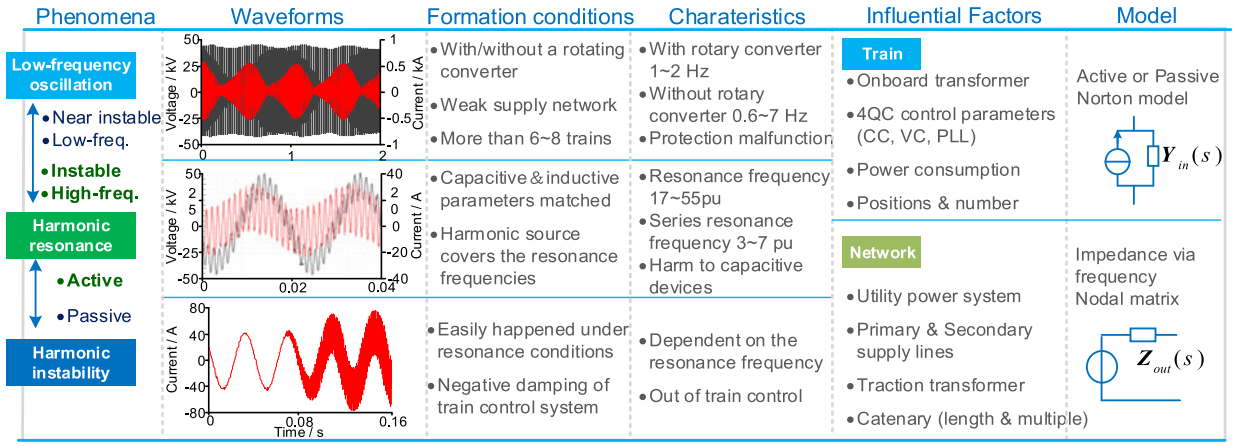

Fig. 9. Overview of the field problems in electric railway systems.

2) Harmonic resonance: happens under the following conditions in electric railways: a) the inductive system with distributed capacitance gives one or more resonance frequencies; b) the harmonic spectra of the HST cover one or more resonance frequencies; c) on the basis of a) and b), the resulted resonances are poorly damped so that the peak driving impedance is relatively steep. Note that the equivalent impedance of the onboard transformer in a train can change the impedance behavior of the traction network seen from the pantograph. Therefore, the equivalent impedance modeling of both HST and traction network in harmonic domain is required.

The total capacitance of the traction network, which is mainly composed of the primary supply line (overhead lines from upstream substation to a traction substation), the secondary supply line (power cables from traction substation to catenary system, about 50–200 m), and the catenary network (overhead lines), is small so that the system resonance frequency may be up to several kilohertz (which means high-order harmonic resonance, exist typically 1–3 kHz).

3) Harmonic instability: Since the harmonic resonance happens in a linearized traction network, the network voltage is highly distorted but still guarantees stable. However, the harmonic instability is an unstable state and can cause overvoltage problems with capacitive devices and arresters [4], the gradually amplified one or more of harmonic components will cause the arrester and protector to explode, electrical equipment overheating, motor failure. With the rapid development of the HSTs, this phenomenon has been a critical power quality issue for electrical railways, especially the HSR. The harmonic instability, which is different from the LFO mainly affected by the low frequency characteristics of the voltage controller (VC) and current controller (CC), is an interactive high-frequency stability problem. Because the harmonic instability is mainly affected by the high-frequency characteristics of the PLL and CC of the electric train output behavior rather than the traction network characteristics. If the train–network closed-loop system has high-frequency unstable poles, the harmonic resonance in network side may increase gradually and lead to harmonic instability.

III. Modeling for the High-Speed Train

Considering the traction units in an HST as a single electrical entry, the most effective way is to formulate restrictions on the input admittance, including the impacts from all the controllers in the 4QC of an HST. It can be done either by defining allowed regions for magnitude and phases, or better for real and imaginary parts of the output admittance. The real part of the output admittance directly determines the damping and/or excitation contribution. It reflects that no instability sources are presented, yet that the instability is always a problem of the interaction behavior [4].

A. Norton-Equivalent Passively Based Model of the HST

The train–network system behaves differently at different frequency bandwidths. Mostly, recent publications regarding harmonic resonance problem have been concentrated on analyzing the former condition without considering the nonlinear loads (NLLs) model or modeling them as a set of ideal current harmonics, which are not comprehensive enough. Many researchers found that the harmonic interaction between network supply voltages and injected current harmonics of NLLs was presented. Nassif *et al.* [31] described several uncoupled or coupled NLL models such as Norton, full model [31], crossed frequency admittance matrix (CFAM) [32], and frequency coupled matrix (FCM) [33] and aimed to present the output behaviors of the NLLs for harmonic studies. The comparison effects of different types of NLL models on the resonance behavior have also been taken into account in [34].

These models based on analytical and measured data can satisfy major of harmonic and harmonic resonance studies in the power system as well as the electric railway system. However, these passively-based NLL models are not applicable when dealing with the instability and oscillation problems of the power converters. One example is that the electric train model was usually replaced by 1–50 pu harmonic current source with 1 pu magnitude in [2] for the analysis of the harmonic propagation and amplification. Alternatively, the harmonic current model of the electric train was established using the measured data

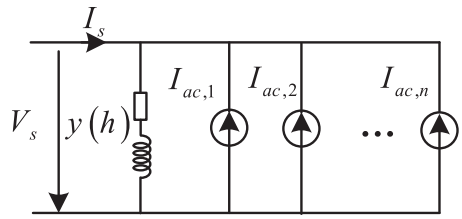

Fig. 10. Norton-equivalent model of a train for harmonic resonance analysis.

and Double Fourier series [35]. Hu *et al*. [36] pointed out that the spectrum of the HST harmonic current has strong randomness and needs to calculate the random harmonic current with a probabilistic method. However, the spectrum distribution of the harmonic current would be influenced by the railway infrastructure, traction network, and operation modes of the train. Thus, this method of simplified modeling cannot reflect the coupled relationship between the 4QCs of HSTs and the traction network, and the output admittance and the participation feature were also ignored.

The Norton model shown in Fig. 10 is usually employed to represent the linear characteristic of the HST in harmonic domain [36]. As the resonance frequencies are usually beyond the switching frequency of the 4QC, it is reasonable to use the passive model of the 4QC for representing the electric train in studying harmonic resonance. The equivalent admittance has passive and active behaviors in terms of considering the effects of the control system. The injected harmonic currents of the train can be presented as

$$\begin{bmatrix} I_s(1) \\ I_s(2) \\ \vdots \\ I_s(n) \end{bmatrix} = \begin{bmatrix} y_s(1) & 0 & 0 & 0 \\ 0 & y_s(2) & 0 & 0 \\ 0 & 0 & \ddots & 0 \\ 0 & 0 & 0 & y_s(n) \end{bmatrix} \times \begin{bmatrix} V_s(1) \\ V_s(2) \\ \vdots \\ V_s(n) \end{bmatrix} - \begin{bmatrix} y_s(1)V_{\mathrm{ac}}(1) \\ y_s(2)V_{\mathrm{ac}}(2) \\ \vdots \\ y_s(n)V_{\mathrm{ac}}(n) \end{bmatrix} \tag{1}$$

where $y_s(h)$, $V_s(h)$ are the harmonic equivalent admittance and harmonic voltage on the secondary side of the traction transformer, respectively; $V_{\mathrm{ac}}(h)$ and $I_{\mathrm{ac}}(h)$ are, respectively, the hth-order harmonic voltage and current of the grid-side of the electric train.

B. Detailed Actively Based Model of the HST

For passive harmonic analysis, $Y_{\mathrm{train}}(s)$ is the admittance of the onboard transformer based on an assumption that the system is stable and the effect of the control system is neglected. However, the passive Norton-equivalent model shown in Fig. 10 has also a limitation for investigating the instability or oscillation problems. Therefore, a detailed model of the train involving variable controllers is considered in this section and called the actively based model.

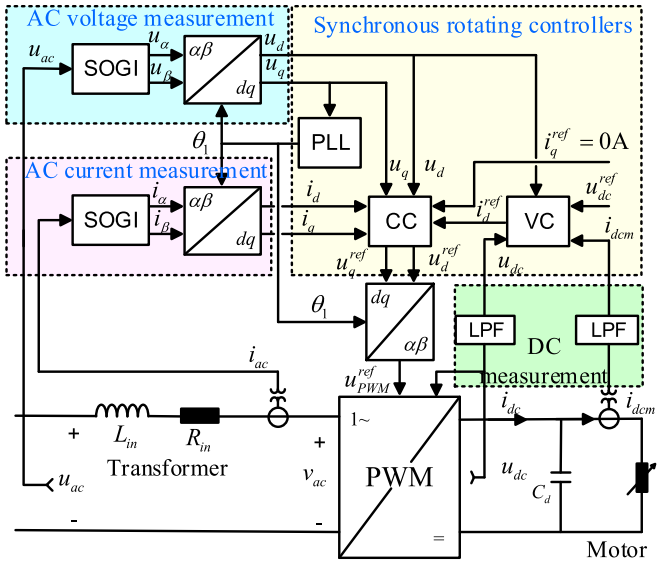

Fig. 11. Control block diagram of the 4QC.

The traction drive system in an HST consists of the onboard transformer, single-phase 4QC, dc link, three-phase inverters, and induction motors [37]. The front-end power converter of HSTs usually adopts a single-phase 4QC to achieve high power factor, low current harmonics, and also bidirectional power-flow capability. The PWM of the 4QC and its control system are of the primary concern for interaction studies, and the detailed control system is shown in Fig. 11.

The active power flow is controlled by the VC, keeping the dc-link voltage u_{dc} to its reference value $u_{\mathrm{dc}}^{\mathrm{ref}}$ by computing the reference active current i_d^{ref} for the CC. Based on the active and reactive current references i_d^{ref} and i_q^{ref} and the network current i_{ac} and voltage u_{ac}, the CC gives the reference voltage $u_{\mathrm{PWM}}^{\mathrm{ref}}$ for the inverter to pulse-width modulate u_{dc} into an ac voltage v_{ac}. This voltage is referred to as the actual voltage since it is this voltage that the vehicle actually controls. The phase angle θ_1 of the input voltage u_{ac} is estimated by the PLL.

Notice that for an ac power system, due to the sinusoidal inputs of ac grids and nonlinear controllers, the input signal may still has the time-varying behavior when using the average model. And these nonlinearities cannot be removed immediately with the standard linearization processes because a well-defined operating point cannot be easily identified. Therefore, a similar impedance-based model is not directly applicable due to their sinusoidal behavior [38]. In order to address the time-varying behavior, dq transformation is used to obtain a nonlinear model with well-defined operating points in the dq frame. Then the system stability can be addressed by the generalized Nyquist stability criterion (GNC). In addition, for the single-phase ac system, the second-order generalized integrator (SOGI) is used to construct a virtual dq component. Therefore, the single-phase ac system with dq decoupling is feasible to apply the small-signal impedance analysis.

The input admittance seen from the electric train in low-frequency range affects the low-frequency voltage variation just

TABLE V
DIFFERENT CONTROLLER FREQUENCY BANDS

Controller	0–10 Hz (Low Fre.)	100 Hz– kHz (Medium High Fre.)	Several kHz (High Fre.)
Voltage controller	√	×	×
Current controller	√	√	√
PLL controller	√	√	√
Feed-forward low pass filter	×	×	√

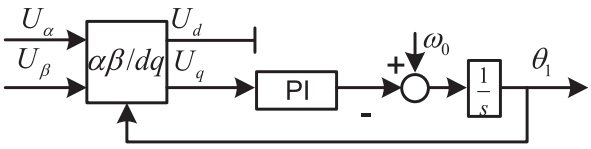

Fig. 12. Block diagram of the PLL.

as the harmonic resonance and instability in high-frequency range. Based on the multi-time scale characteristics of the VSC control system [39], the 4QC system adopts current controller with about 50–1000 Hz bandwidth and excited voltage or/and power controllers with about 10–100 Hz bandwidth. The dynamic characteristics of the different controllers are listed in Table V. Note that the dynamic characteristics in different frequency bands are closely related to the corresponding controller parameters.

1) Phase-Locked Loop: The PLL acts as a synchronization control loop whose main function is to make the network voltage and current in same phase, which means that the power factor is close to the per unit. The synchronization angle θ_1 from the PLL is used for $\alpha\beta$/dq transformation in the 4QC control system. It can be found that there are two synchronous rotating frames, i.e., the network dq frame and the 4QC dq frame. In this paper, the subscript c and g are adopted for distinguishing the 4QC dq frame and the network dq frame; for instance, the voltage vector $\mathbf{U}_g$ and current vector $\mathbf{I}_g$ belong to the network dq frame and $\mathbf{U}_c$ and $\mathbf{I}_c$ are in the 4QC dq frame. The block diagram of the PLL is shown in Fig. 12.

The following relationship exists between the stationary $\alpha\beta$ frame and dq frame [40]:

$$\mathbf{U}_{\alpha\beta} = e^{j\theta}\mathbf{U}_g, \quad \mathbf{U}_{\alpha\beta} = e^{j\theta_1}\mathbf{U}_c, \qquad \theta = \theta_1 + \Delta\theta. \quad (2)$$

The error angle $\Delta\theta$ is zero in the steady state. There will be a phase-locked error owing to occur a small disturbance at steady-state operating point, giving

$$\mathbf{U}_c = e^{-j\Delta\theta}\mathbf{U}_g. \quad (3)$$

Equation (3) can be linearized as

$$\mathbf{U}_c \approx (1 - j\Delta\theta)(U_{d0} + \Delta\mathbf{U}_g) \approx U_{d0} + \Delta\mathbf{U}_g - jU_{d0}\Delta\theta$$
$$\Rightarrow \mathrm{Im}(\mathbf{U}_c) = \mathrm{Im}(\Delta\mathbf{U}_g) - U_{d0}\Delta\theta \quad (4)$$

where U_{q0} is equal to zero in steady state for a unit power factor. From Fig. 11, the phase-locked error can be expressed as

$$s\theta_1 = [\omega_0 - F_{\mathrm{PLL}}(\mathrm{s})\mathrm{Im}(\mathbf{U}_c)]$$
$$\Rightarrow s\Delta\theta = \omega_0 - s\theta_1 = F_{\mathrm{PLL}}(\mathrm{s})\mathrm{Im}(\mathbf{U}_c) \quad (5)$$

where $F_{\mathrm{PLL}}(s) = Kp_{\mathrm{PLL}} + Ki_{\mathrm{PLL}}/s$ is the transfer function of the PI controller in the PLL. ω_0 is the fundamental angular frequency, $\omega_0 = s\theta$. Combining (2) to (5), one can obtain the following equation:

$$s\theta = w_0 + F_{\mathrm{PLL}}(s)s(\theta - \theta_1) \Rightarrow \Delta\theta$$
$$= \underbrace{\frac{F_{\mathrm{PLL}}(s)}{s + U_{d0}F_{\mathrm{PLL}}(s)}}_{G_{\mathrm{PLL}}(s)}\mathrm{Im}(\Delta\mathbf{U}_g) \quad (6)$$

where $F_{\mathrm{PLL}}(s) = Kp_{\mathrm{PLL}} + Ki_{\mathrm{PLL}}/s$ is the transfer function of the PI controller in the PLL. Inserting (6) into (4), the transfer function in matrix form of the PLL can be obtained by

$$\begin{bmatrix}\Delta U_d^c \\ \Delta U_q^c\end{bmatrix} = \underbrace{\begin{bmatrix}1 & 0 \\ 0 & 1 - U_{d0}G_{\mathrm{PLL}}(s)\end{bmatrix}}_{G_{u\,\mathrm{PLL}}(s)}\begin{bmatrix}\Delta U_d^g \\ \Delta U_q^g\end{bmatrix}. \quad (7)$$

Correspondingly, the transfer function of the current synchronization system can be expressed as

$$\begin{bmatrix}\Delta I_d^c \\ \Delta I_q^c\end{bmatrix} = \begin{bmatrix}\Delta I_d^g \\ \Delta I_q^g\end{bmatrix} - \underbrace{\begin{bmatrix}0 & I_{q0}G_{\mathrm{PLL}}(s) \\ 0 & I_{d0}G_{\mathrm{PLL}}(s)\end{bmatrix}}_{G_{i\,\mathrm{PLL}}(s)}\begin{bmatrix}\Delta U_d^g \\ \Delta U_q^g\end{bmatrix} \quad (8)$$

where $I_{d0} = P_0/U_{d0}$ and $I_{q0} = Q_0/U_{d0}$ are the steady-state active and reactive currents. P_0 and Q_0 are the output active power and the reactive power of the 4QC, respectively.

2) Current Controller: Applying the law of Kirchhoff in Fig. 11, the input voltage of the 4QC in the network *dq* frame is given by

$$\boldsymbol{V_g} = \boldsymbol{U_g} - \boldsymbol{I_g}[R_{\mathrm{in}} + (s + j\omega_0)L_{\mathrm{in}}]. \quad (9)$$

Equation (9) can be transformed to the 4QC dq frame, following the conversion relationship between the 4QC dq frame and the network dq frame in (2), yields:

$$\begin{bmatrix}v_d^c \\ v_q^c\end{bmatrix} = \begin{bmatrix}u_d^c \\ u_q^c\end{bmatrix} - \begin{bmatrix}R_{\mathrm{in}} + sL_{\mathrm{in}} & -\omega_0 L_{\mathrm{in}} \\ \omega_0 L_{\mathrm{in}} & R_{\mathrm{in}} + sL_{\mathrm{in}}\end{bmatrix}\begin{bmatrix}i_d^c \\ i_q^c\end{bmatrix}. \quad (10)$$

The decoupling is added to the control loop in the form of an inner positive-feedback loop with gain $w_0 L_{\mathrm{in}}$. From Fig. 13, the voltage reference matrix $\mathbf{U}^{\mathrm{ref}}$ can be derived as

$$\begin{bmatrix}u_d^{\mathrm{ref}} \\ u_q^{\mathrm{ref}}\end{bmatrix} = \begin{bmatrix}u_d^c \\ u_q^c\end{bmatrix} - F_{CC}(s)\begin{bmatrix}i_d^{\mathrm{ref}} - i_d^c \\ i_q^{\mathrm{ref}} - i_q^c\end{bmatrix} - \begin{bmatrix}0 & -\omega_0 L_{\mathrm{in}} \\ \omega_0 L_{\mathrm{in}} & 0\end{bmatrix}\begin{bmatrix}i_d^c \\ i_q^c\end{bmatrix} \quad (11)$$

where $F_{\mathrm{CC}}(s) = Kp_{\mathrm{CC}} + Ki_{\mathrm{CC}}/s$ is the transfer function of the CC.

The output voltage signal of the CC is the input of the PWM controller. If the PWM delay and computation delay are consid-

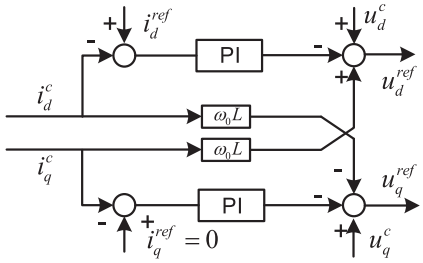

Fig. 13. Block diagram of the current controller.

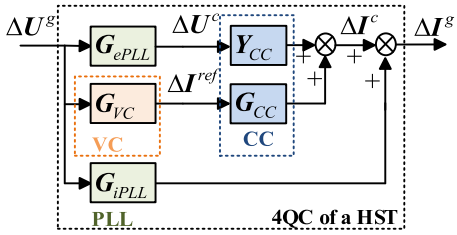

Fig. 14. Small-signal linearization block diagram of the 4QC control system of an HST.

ered, we have

$$\begin{bmatrix} v_d^c \\ v_q^c \end{bmatrix} = G_d(s) \begin{bmatrix} u_d^{\mathrm{ref}} \\ u_q^{\mathrm{ref}} \end{bmatrix}, \qquad G_d(s) = \frac{1}{T_d s + 1} \tag{12}$$

where the time delay $G_d(s)$ is the first-order process, $T_d = 1.5T_s$, and T_s is the sampling time [41].

Combining (9) to (12), the small-signal-based transfer function of the CC in the *dq* frame can be expressed as

$$\begin{bmatrix} \Delta i_d^c \\ \Delta i_q^c \end{bmatrix} = \mathbf{G}_{\mathrm{CC}}(s) \begin{bmatrix} \Delta i_d^{\mathrm{ref}} \\ \Delta i_q^{\mathrm{ref}} \end{bmatrix} + \mathbf{Y}_{\mathrm{CC}}(s) \begin{bmatrix} \Delta u_d^c \\ \Delta u_q^c \end{bmatrix} \tag{13}$$

where $\mathbf{G}_{\mathrm{CC}}(s)$ and $\mathbf{Y}_{\mathrm{CC}}(s)$ are the transfer function and input admittance of the CC, respectively. Equation (14) shown at the bottom of this page.

3) Voltage Controller: The VC needs to provide the active current reference signal I_d^{ref} for the CC by power conservation principle, which called double voltage and current closed-loop control. The voltage vector and the current vector of different coordinate systems are equally in steady state, i.e., $\mathbf{U}_g = \mathbf{U}_c$ and $\mathbf{I}_g = \mathbf{I}_c$. Setting $\mathbf{U}_g$ as a phase reference, if there is a small disturbance around the steady-state operating point, the network voltage and current are giving by

$$\begin{cases} \mathbf{U}_g = U_{d0} + \Delta U_d^g + j\Delta U_q^g \\ \mathbf{I}_g = I_{d0} + \Delta I_d^g + j(I_{q0} + \Delta I_q^g) \end{cases}. \tag{15}$$

Thus, the instantaneous active and reactive powers at the network side of the 4QC can be expressed as

$$\begin{cases} P = \mathrm{Re}(\mathbf{U}_g \mathbf{I}_g) \approx \underbrace{U_{d0} I_{d0}}_{P_0} + \underbrace{I_{d0}\Delta U_d^g + I_{q0}\Delta U_q^g + U_{d0}\Delta I_d^g}_{\Delta P} \\ Q = \mathrm{Im}(\mathbf{U}_g \mathbf{I}_g) \approx \underbrace{-U_{d0} I_{q0}}_{Q_0} + \underbrace{I_{d0}\Delta U_q^g - I_{q0}\Delta U_d^g + U_{d0}\Delta I_q^g}_{\Delta Q} \end{cases}. \tag{16}$$

Assuming that the switching process of the 4QC is ideal and lossless, the powers between ac side and dc side satisfy the following relationship:

$$u_d^g i_d^g + u_q^g i_q^g = \frac{1}{2} \cdot C_d \frac{du_{\mathrm{dc}}^2}{dt} + \frac{u_{\mathrm{dc}}^2}{R_L}. \tag{17}$$

The VC is a simple proportional–integral (PI) control, and the main task of the VC is to keep the dc-link voltage u_{dc} following its reference value $u_{\mathrm{dc}}^{\mathrm{ref}}$. The transfer function of the VC is

$$i_d^{ref} = F_{\mathrm{VC}}(s) \cdot (u_{\mathrm{dc}}^{\mathrm{ref}} - u_{\mathrm{dc}}) \tag{18}$$

where $F_{\mathrm{VC}}(s) = Kp_{\mathrm{VC}} + Ki_{\mathrm{VC}}/s$ is the transfer function of the VC. Harnefors *et al.* [40] introduced the modeling method of the VC. Based on this method, after linearizing (17) and (18), the small-signal transfer function of the VC can be derived as

$$\begin{bmatrix} \Delta i_d^{\mathrm{ref}} \\ \Delta i_q^{\mathrm{ref}} \end{bmatrix} = \underbrace{\begin{bmatrix} -G_{\mathrm{dc}}^d(s) & G_{\mathrm{dc}}^q(s) \\ 0 & 0 \end{bmatrix}}_{\mathbf{G}_{\mathrm{VC}}(s)} \begin{bmatrix} \Delta u_d^g \\ \Delta u_q^g \end{bmatrix} \tag{19}$$

where the elements of $\mathbf{G}_{\mathrm{VC}}(s)$ can be expressed as

$$G_{\mathrm{dc}}^d(s) = \frac{\left[\mathbf{Y}_{\mathrm{CC}}(1,1) + \frac{P_0}{U_{d0}^2} - \frac{P_0}{U_{d0}^2}\mathbf{G}_{\mathrm{CC}}(1,1)\right] F_{\mathrm{VC}}(s)}{sC_d + \mathbf{G}_{\mathrm{CC}}(1,1) F_{\mathrm{VC}}(s)} + \frac{P_0}{U_{d0}^2} \tag{20}$$

$$G_{\mathrm{dc}}^q(s) = \frac{\left[Q_0 - U_{d0}^2 \mathbf{Y}_{\mathrm{CC}}(1,2)\right] F_{\mathrm{VC}}(s)}{U_{d0}^2 \left[sC_d + \mathbf{G}_{\mathrm{CC}}(1,1) F_{\mathrm{VC}}(s)\right]}. \tag{21}$$

Combining (7), (8), (13), and (19), based on the aforementioned analysis, the small-signal linearization block diagram of train's 4QC control system can be obtained in Fig. 14.

$$\begin{cases} \mathbf{G}_{\mathrm{CC}}(s) = \mathbf{H}_{dq}^{-1} \begin{bmatrix} G_d(s) F_{\mathrm{CC}}(s) & 0 \\ 0 & G_d(s) F_{\mathrm{CC}}(s) \end{bmatrix} \\ \mathbf{Y}_{\mathrm{CC}}(s) = \mathbf{H}_{dq}^{-1} \begin{bmatrix} 1 - G_d(s) & 0 \\ 0 & 1 - G_d(s) \end{bmatrix} \\ \mathbf{H}_{dq}^{-1} = \begin{bmatrix} G_d(s) F_{\mathrm{CC}}(s) + R_{\mathrm{in}} + sL_{\mathrm{in}} & (\omega_0(1 - G_d))L_{\mathrm{in}} \\ -(\omega_0(1 - G_d))L_{\mathrm{in}} & G_d(s) F_{\mathrm{CC}}(s) + R_{\mathrm{in}} + sL_{\mathrm{in}} \end{bmatrix} \end{cases} \tag{14}$$

The input admittance matrix of the electric train, including the CC, VC, and PLL, is expressed as

$$\Delta \mathbf{I}^g(s) = [\mathbf{G}_{\mathrm{CC}}\mathbf{G}_{\mathrm{VC}} + \mathbf{Y}_{\mathrm{CC}}\mathbf{G}_{u\mathrm{PLL}} + \mathbf{G}_{i\mathrm{PLL}}]\,\Delta \mathbf{U}^g(s)$$
$$\Rightarrow \begin{bmatrix} \Delta i_d^g(s) \\ \Delta i_q^g(s) \end{bmatrix} = \underbrace{\begin{bmatrix} Y_{dd}(s) & Y_{dq}(s) \\ Y_{qd}(s) & Y_{qq}(s) \end{bmatrix}}_{\mathbf{Y}_{\mathrm{train}}(s)} \begin{bmatrix} \Delta u_d^g(s) \\ \Delta u_q^g(s) \end{bmatrix} \tag{22}$$

where $\mathbf{G}_{u\mathrm{PLL}}(s)$ and $\mathbf{G}_{i\mathrm{PLL}}(s)$ represent the voltage and the current transfer function of the PLL, respectively. $\mathbf{Y}_{\mathrm{CC}}(s)$ and $\mathbf{G}_{\mathrm{CC}}(s)$ are the input admittance and the transfer function in the CC, respectively. $\mathbf{G}_{\mathrm{VC}}(s)$ represents the transfer function of the VC.

IV. Traction Network Modeling

Different from the analysis method of the LFO and harmonic instability, the harmonic resonance depends more information about the network topology and its parameter, and also represents the train as a passive harmonic model. Therefore, a detailed network model, including all network components, is built in this section for analyzing the influential factors of the harmonic resonance.

A. Equivalent Traction Network Model for LFO and Harmonic Instability Analysis

The all-parallel AT-fed catenary system is generally adopted in China HSR. The mathematical model of the traction network mainly contains the equivalent circuit model, generalized symmetrical component model, and chain-circuit model [42]. The equivalent circuit model with resistance–inductance is widely used for tuning the control of inverters and studying the control performance [43]. For a single-phase ac system, the voltage drop over a resistor R_s and an inductor L_s can be described as

$$\begin{cases} u_S(t) - u_{\mathrm{ac}}(t) = R_s \cdot i(t) + L_s \frac{di(t)}{dt} \\ i(t) = i_d \cos(\omega_0 t) - i_q sin(\omega_0 t) \end{cases} \tag{23}$$

where $u_s(t)$ is the output voltage of the traction substation, $u_{\mathrm{ac}}(t)$ is the input voltage of the electric train, and $i(t)$ is the network current. Transforming (23) into the dq reference frame, the network voltage dynamic is given by

$$\begin{bmatrix} \Delta u_d^g(s) \\ \Delta u_q^g(s) \end{bmatrix} = \underbrace{\begin{bmatrix} R_s + sL_s & -\omega_0 L_s \\ \omega_0 L_s & R_s + sL_s \end{bmatrix}}_{\mathbf{Z}_s(s)} \begin{bmatrix} \Delta i_d^g(s) \\ \Delta i_q^g(s) \end{bmatrix} \tag{24}$$

where Δ denotes the small deviation of the respective variable from the equilibrium point and s is the Laplace operator d/dt. ω_0 is the fundamental angular frequency and R_s and L_s are the equivalent resistance and inductance of the network, respectively. $\mathbf{Z}_s(s)$ is the required equivalent impedance of the traction network. In order to investigate the interaction behaviors of the traction network and HST system in a same voltage level, one can convert the network voltage and impedance at the primary side of the 4QC in the HST to its secondary side, i.e., $Z_S^* = Z_S/k^2$, where k is the onboard transformer ratio.

B. Detailed Traction Network Model

The essential elements of the traction power supply system are traction substation (TSS), autotransformers (ATs), traction lines (including contact wires (CWs), messenger wires (MWs), feeders, protect wires (PWs), integrated ground lines (IGLs), rails). The utility power system supplies 220 kV source to the TSS that are step down to 2×27.5 kV by the V/x traction transformers in the TSS. The traction lines are 2×27.5 kV AT-fed traction network and they connect to the same type wires though crossing wires (CW) in ATs and section posts (SPs), which installed approximately every 10–15 km along the track.

1) Traction Transformers: The model of the traction transformer installed in the traction substation has been widely presented in the previous work [3]. V/x connection transformer is the most popular type in China HSRs for its simple connection, high-capacity utilization, and better solution of the unbalance problem. The model of this transformer can be found in [3]. Alternatively, [2] also proposed a simulation model for Scott-connection transformer widely adopted in Korea. The numerous models of representative traction transformers, such single-phase, V/v, Scott and Balanced transformer, can be found in [44]. Moreover, the modeling for the AT is similar to the traditional autotransformers [45]. The aforementioned electrical modeling of different traction electric devices is combined in a unified system in terms of a nodal admittance matrix, which is used to study the low-frequency and high-frequency electrical characteristics.

2) Capacitance and Impedance of the Traction Conductors: The traction line that contains up and down tracks is analyzed by a five-conductor model. It contains up contact wire, up feeder, rail, down contact wire and down feeder. The catenary structure is different with various geographical conditions, leading to different parameters and algorithms in the traction conductors model. The self- and mutual impedances of conductors can be calculated with complex depth equation in (25) [46], [47]

$$Z_{\mathrm{ii}} = j\omega \frac{\mu_0}{2\pi} \ln \frac{2\,\mathrm{h}_i}{r_i} + 2\,(\Delta R_{\mathrm{ii}} + j\Delta X_{\mathrm{ii}})\,,$$
$$Z_{\mathrm{ij}} = j\omega \frac{\mu_0}{2\pi} \ln \frac{D_{\mathrm{ii}}}{d_{\mathrm{ij}}} + 2\,(\Delta R_{\mathrm{ij}} + j\Delta X_{\mathrm{ij}}) \tag{25}$$

where the first item in (25) is line impedance in the case of ideal earth. The second item is the correction item when the earth is not ideal. Additionally, the correction item is an infinite integral from in the traditional Carson model.

As to the self- and mutual admittances of conductors, the potential coefficient can be obtained by (26)

$$p_{\mathrm{ii}} = \frac{1}{2\pi\varepsilon_0} \ln \frac{2\,\mathrm{h}_i}{r_{\mathrm{eq}}}\ (\mathrm{F/m})^{-1},\ \ p_{\mathrm{ij}} = \frac{1}{2\pi\varepsilon_0} \ln \frac{D_{\mathrm{ij}}}{d_{\mathrm{ij}}}\ (\mathrm{F/m})^{-1} \tag{26}$$

where p_{ii} and p_{ij} are the self- and the mutual potential coefficients, respectively. And, ε_0 is the permittivity of vacuum, $\varepsilon_0 = 8.854188 \times 10^{-12}$(F/m). The structural parameters in (25) and (26) are illustrated in Fig. 15. The capacitance matrix can be derived from the inverse matrix of the potential coefficient matrix $\mathbf{P}$, given as $\mathbf{C} = \mathbf{P}^{-1}$. The admittance matrix of the traction network conductors is $\mathbf{Y} = j2\pi f \cdot \mathbf{C}$.

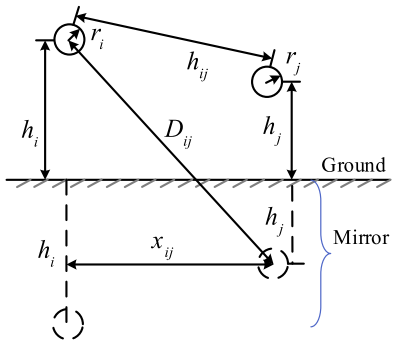

Fig. 15. Conductor geographical structure.

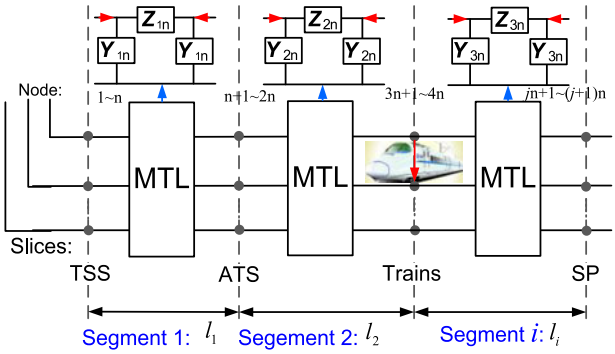

Fig. 16. Schematic of traction MTL segments.

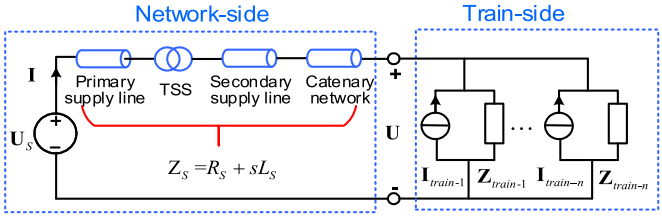

Fig. 17. Impedance-based analysis of the network system and train system.

3) Multiple Transmission Line Model for the Catenary Network: The catenary network is another important component in studying the train–network interaction. The multiple catenary network conductors can be regarded as one symmetrical linear and passive multiport network. A multiple transmission line (MTL) model is widely accepted for modeling different segments of the catenary network conductors, which is illustrated in Fig. 16.

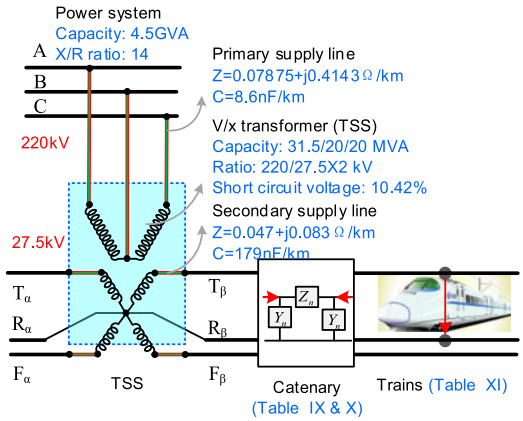

Fig. 18. Sketch of the train–network simulation model.

Each segment is represented by a Π-equivalent circuit matrix with $2n \times 2n$ elements. The segments of the catenary network are resulted from the slices of the dynamic positions of running trains and fixed positions of AT substations, SPs, and traction substations. Moreover, these catenary conductors can be represented as parallel transmission lines with self- and mutual impedances and admittances, and these parameters are frequency dependent due to skin effect. With some assumptions in [48], the MTL can be obtained by a set of partial different equations in time domain [see (27)]

$$\left.\begin{aligned} \frac{\partial}{dx}\mathbf{V}(x,t) &= -\mathbf{R}\mathbf{I}(x,t) - \mathbf{L}\frac{\partial}{\partial t}\mathbf{I}(x,t) \\ \frac{\partial}{\partial x}\mathbf{I}(x,t) &= -\mathbf{G}\mathbf{I}(x,t) - \mathbf{C}\frac{\partial}{\partial t}\mathbf{V}(x,t) \end{aligned}\right\} \tag{27}$$

where $\mathbf{V}$ is the voltage vector between the catenary conductors and the earth, $\mathbf{I}$ is the current vector through the catenary conductors, and $\mathbf{R}$, $\mathbf{L}$, $\mathbf{G}$, and $\mathbf{C}$ are the $2n \times 2n$ matrices of line parameters per unit length. Based on the eigenvalues decomposition, one can get

$$\mathbf{ZY} = \mathbf{T}^{-1}\mathbf{\Lambda}\mathbf{T} \tag{28}$$

where $\mathbf{Z}$ and $\mathbf{Y}$ are the impedance matrix and the admittance matrix of an MTL, respectively; and $\mathbf{Z} = \mathbf{R} + jh\omega\mathbf{L}$, $\mathbf{Y} = \mathbf{G} + jh\omega\mathbf{C}$, h is the harmonic order, and ω is the fundamental angular frequency.

Each section can be equivalent to a multiconductor Π-type circuit where $\mathbf{Z}_L$ represents the impedance matrix and $\mathbf{Y}_L/2$ represents the admittance matrix, as shown in Fig. 16. $\mathbf{Z}_L$ and $\mathbf{Y}_L/2$, $2n \times 2n$ complex symmetric matrices, can be obtained

$$\mathbf{Y}_{\text{net}} = \begin{bmatrix} \mathbf{Y}_{1n} + \mathbf{Z}_{1n}^{-1} & -\mathbf{Z}_{1n}^{-1} & & & \\ -\mathbf{Z}_{1n}^{-1} & \mathbf{Z}_{1n}^{-1} + \mathbf{Y}_{2n} + \mathbf{Z}_{2n}^{-1} & & & \\ & \ddots & \ddots & \ddots & \\ & & \mathbf{Z}_{(N-2)n}^{-1} + \mathbf{Y}_{(N-1)n} + \mathbf{Z}_{(N-1)n}^{-1} & -\mathbf{Z}_{(N-1)n}^{-1} \\ & & -\mathbf{Z}_{(N-1)n}^{-1} & \mathbf{Z}_{(N-1)n}^{-1} + \mathbf{Y}_{Nn} \end{bmatrix} \tag{30}$$

TABLE VI
TYPICAL IMPEDANCE RATIO OF EACH NETWORK COMPONENT

Classification	Total Impedance (Ω)	Utility	Primary Line	Transformer	Secondary Line	Catenary
Conventional railway	30.52	8.3%	4.6%	41.3%	0.0%	45.8%
High speed railway	15.14	2.2%	9.3%	33.0%	0.1%	55.4%

Note: The length of the primary line, the secondary line, and catenary are set as 5 km, 100 m, and 25 km, respectively.

TABLE VII
DYNAMICS OF THE 4QC UNDER DIFFERENT FREQUENCY WIDTHS

Frequency Width	Low Frequency	Medium High Frequency	High Frequency
Problems	Low Frequency Oscillation	Harmonic Instability	Harmonic Resonance
Characteristic equation	$\mathbf{G}_{ol}(s)=\mathbf{I}+n\mathbf{Y}_{\text{train}}(s)\mathbf{Z}_S(s)$	$\mathbf{G}_{ol}(s)=\mathbf{I}+n\mathbf{Y}_{\text{train}}(s)\mathbf{Z}_S(s)$	×
Criterion	Generalized Nyquist criterion: $n\mathbf{Z}_S(s)\mathbf{Y}_{\text{train}}(s)$	Generalized Nyquist criterion: $n\mathbf{Z}_S(s)\mathbf{Y}_{\text{train}}(s)$	×
Dynamics part	VC, PLL, CC	PLL, CC, T_d	×

Note: VC is the outer voltage controllers, CC is the inner current controller, PLL is the phase-locked loop, and T_{d} is time delay.

by (29) through the phase-mode transformation

$$\begin{cases}\mathbf{Z}_L=\mathbf{T}\left[\mathbf{\Lambda}^{-1/2}\sin h\left(\mathbf{\Lambda}^{-1/2}\times l\right)\right]\mathbf{T}^{-1}\mathbf{Y}^{-1}\\ \mathbf{Y}_L/2=\mathbf{Z}^{-1}\mathbf{T}\left[\mathbf{\Lambda}^{-1/2}\tan h\left(\mathbf{\Lambda}^{-1/2}\times l/2\right)\right]\mathbf{Y}^{-1}\end{cases}\tag{29}$$

where l is the length of an MTL segment.

Finally, the whole traction network can be modeled in a unified modal matrix with jointing all segments. Each section cut by these slices could be regarded as a passive and homogeneous multiconductor transmission line. Therefore, the equivalent node–admittance matrix can be described by (30) through a series of MTL matrices in Fig. 16. Equation (30) shown at the bottom of previous page.

The nodal injection current of the catenary network is composed of these slices

$$\mathbf{I}_{\text{net}}=\left[\mathbf{I}_1\ \mathbf{I}_2\ \cdots\ \mathbf{I}_{N-1}\ \mathbf{I}_N\right]_h^T.\tag{31}$$

The injection current vectors change with the state of mutational slices. Taking the location of a train as an example, if the slice *i* represents the location of an HST, the current vector in this slice is not zero vector. Otherwise, if the HST is located on the up track, then $\mathbf{I}_i=\left[-I_i^{\text{train}}\ 0\ I_i^{\text{train}}\ 0\ 0\right]_h^T$, else $\mathbf{I}_i=\left[0\ 0\ I_i^{\text{train}}\ -I_i^{\text{train}}\ 0\right]_h^T$.

4) Impedance Ratio of Each Network Components: A Simple Case: The traction network subsystem includes the utility power grid, primary/secondary supply lines, traction transformer, catenary lines, and autotransformers. Majority of the traction network elements is resistive–inductive in the low-frequency region, while the presence of secondary supply lines and catenary conductors are mainly capacitive in higher frequency region. The detailed traction conductors' parameters and their types can be found in Fig. 18. In order to practically assess the approximate effects of the main electrical elements in harmonic resonance, LFO, and harmonic instability, we listed the typical impedance values and their ratios of the total impedance in Table VI. The impedance ratio represents the ratio of the impedance of each component to the total impedance of the network. Therefore, for a conventional railway, the impedance ratio of the utility grid, primary supply line, transformer, secondary supply line, and catenary lines will be about 8.3%, 4.6%, 41.3%, 0.0% and 45.8%. For the HSR (220 kV, 4.5 GVA), the impedance ratios will be about 2.2%, 9.3%, 33.0%, 0.1% and 55.4%, respectively. Table VI summarizes these parameters, and they can be practical for assessing and mitigating the power quality phenomena. The impedance ratios of different elements also affect their influential degrees on the harmonic resonance and oscillations.

V. TRAIN–TRACTION NETWORK INTERACTION MODEL

Many power delivery and harmonic distortion problems in traction system are due to interactions between the traction network and the electric trains. Fig. 17 shows the impedance-based diagram of the train–network system.

In this study, the LFO and the instability problem are paid attention to from the point of the system. Therefore, only inner current controller, outer voltage/power controller, PLL, and related parameters are taken into consideration. In addition, according to the characteristic of multi-time-scale characteristic in the control system of inverter [39], it is necessary to consider the low-frequency, medium high-frequency, high-frequency, and the corresponding dynamic components, as shown in Table VII.

From Table VII, there are four factors that need to be considered in the detail impedance model.

1) the total time delay T_{d}, i.e., computation-plus-PWM;
2) the PLL;
3) the inner current control dynamics;
4) the dynamics behaviors of the outer power/voltage controllers, i.e., the voltage control and power control, provided that such are used, for the reactive power or the point-of-common-coupling (PCC) voltage magnitude.

Causes 1), 2) and 3) affect the harmonic instability, whereas causes 3) and 4) affect the LFOs.

A. Generalized Simulation Model for Case Studies

A generalized simulation model, consisting of the power utility system, the traction system, and trains, is presented for

TABLE VIII
MAJOR PARAMETERS OF POWER SYSTEM, TRACTION TRANSFORMER, AND AT TRANSFORMER

Components	Parameters	Values
V/x transformer	Nominal capacity (MVA)	31.5/20/20
	Ratio (kV/kV)	220/2×27.5
	Impedance voltage	10.42%
	Load loss (kW)	141.76
AT transformer	Nominal capacity (MVA)	16
	Ratio (kV/kV)	55/27.5
	Impedance voltage	1.7%
	Load loss (kW)	56.412
	No-load loss (kW)	11.313
	No-load current	0.071%

TABLE IX
TRACTION NETWORK IMPEDANCE AT 50 HZ (Ω km)

	T_1	F_1	R	T_2	F_2
T_1	0.0781 + 0.6203i	0.0501 + 0.3276i	0.0497 + 0.3193i	0.0484 + 0.3357i	0.0482 + 0.3002i
F_1	0.0501 + 0.6376i	0.0956 + 0.7361i	0.0539 + 0.3185i	0.0482 + 0.3002i	0.0485 + 0.2862i
R	0.0497 + 0.3193i	0.0539 + 0.3185i	0.0568 + 0.3991i	0.0497 + 0.3193i	0.0539 + 0.3185i
T_2	0.0484 + 0.3357i	0.0482 + 0.3002i	0.0495 + 0.3193i	0.0781 + 0.6203i	0.0501 + 0.3276i
F_2	0.0482 + 0.3002i	0.0485 + 0.2862i	0.0485 + 0.3184i	0.0501 + 0.3276i	0.0956 + 0.7361i

TABLE X
TRACTION NETWORK CAPACITANCE AT 50 HZ (NF/KM)

	T_1	F_1	R	T_2	F_2
T_1	12.02	1.14	3.64	1.86	0.37
F_1	1.14	8.75	3.74	0.37	0.14
R	3.64	3.47	67.23	3.64	3.47
T_2	1.86	0.37	3.64	12.02	1.14
F_2	0.37	0.14	3.47	1.14	8.75

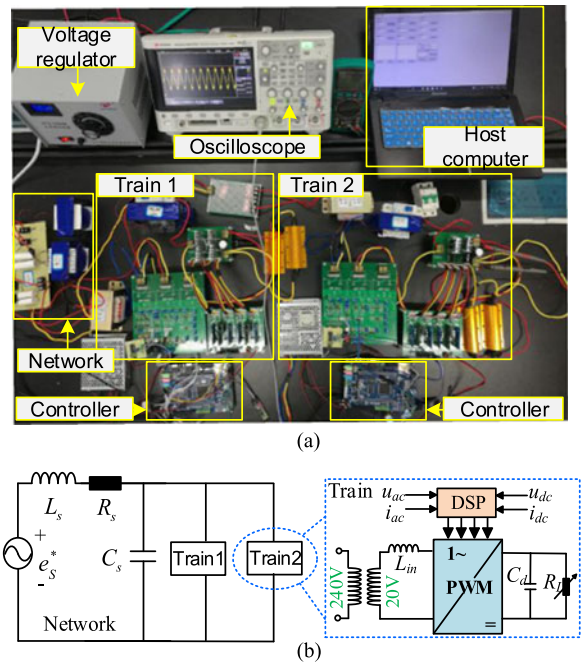

Fig. 19. Experimental platform of the multi-train and network model for LFO and harmonic instability studies: (a) circuit diagram; (b) platform diagram.

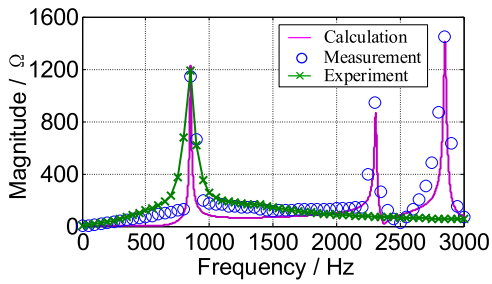

Fig. 20. Impedance via frequency curve of the traction network. Red solid line: calculation results; blue circle: simulation results; green fork line: experiment results.

evaluating the interactions between the trains and the traction network. The parameters are listed in Fig. 18 and Table VIII–X.

B. Generalized Experiment Platform for Case Studies

A scaled down experimental platform with multiple trains and network system is carried out. The hardware picture is shown in Fig. 19. Where L_s and R_s represent the equivalent impedance between the first train and the power source. C_s is the network equivalent capacitance, which is used to construct the resonant point. The main circuit and controller structures of trains are the same with the simulation model, but the parameters of the experimental system in Fig. 19 have different values with the simulation example. In the experimental system, the source is ac 240 V, the switching frequency is set at 1250 Hz, and the control system of 4QC is implemented into DSP (TMS320F28335). The high-speed 12-bit A/D board, DSO-X3034A, is used for sampling the voltage and currents, and the digital wave-form output board, TX-DA962D4, is used for the PWM generation. In addition, a custom docking board with voltage and current sensing was designed.

C. Impedance-Based Train–Network Model Validation

In order to validate the mathematical model, a generalized simulation model and an experimental platform have been conducted. The impedance behaviors of the traction network and HSTs have been compared with the simulation results. Here, the frequency-scanning method is used for the computing impedance of the simulation results.

1) Traction Network Impedance Validation: Fig. 20 shows the utility test results of traction network impedance versus frequency through the frequency-scanning method. In this case, the traction network modeled in Section IV-B consists of the power system, primary supply line, V/x transformer, secondary supply line, and multiple transmission lines. This structure is

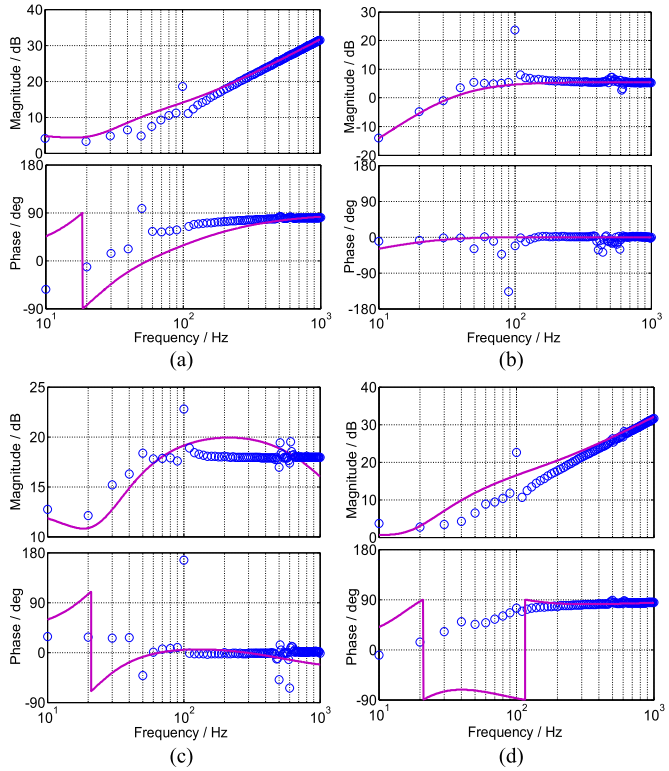

Fig. 21. Calculated and simulation impedance via frequency curve of the train. Red solid line: calculated results. Blue circle: simulation results. (a) Z_{dd}; (b) Z_{dq}; (c) Z_{qd}; (d) Z_{qq}.

similar to the simulation model in Fig. 18, and the parameters listed in Table VIII–X. Meanwhile, the test frequency is from 50 Hz to 3 kHz and the step is 50 Hz. The impedance via the frequency curve of the traction network is shown in Fig. 20, where the red solid lines are the calculation results, the blue circles '○' are the simulation results and the green fork lines depict the experiment results. The simulation results matched well with the mathematical method. It is valid that the simulation system can represent the critical resonance and can be applied for the case studies. The experiment system includes a simple *RLC* circuit for representing the critical resonance points and low-frequency impedance. It is indicated that the simulation and experiment systems are reliable and valid to perform the works and case studies of this paper.

2) Train Impedance Validation: In order to validate the proposed calculated impedance model of the 4QC of the HST, the frequency-scanning method is applied. The impedance frequency responses of the 4QC in the simulation system is measured from 25 to 1000 Hz and the step is 25 Hz. Fig. 21 depicts the simulation impedance frequency responses over-plotted with calculated results using (22) for unit power factor control. The parameters are listed in Table XI, and the load resistance of train is set as $R_L = 5\ \Omega$. In Fig. 21, the red solid line is from calculated and the blue circle '○' are from simulation measured. The results show a good accuracy of the proposed impedance model of the train. As a result, the train–network simulation and experiment systems can be able to study the harmonic and instability problems mentioned earlier.

TABLE XI
PARAMETERS OF THE TRAIN–NETWORK SYSTEM FOR LFO AND HARMONIC INSTABILITY ANALYSIS

Symbol	Description	Simulation Value	Experiment Value
e_S^*	Secondary side voltage of the onboard transformer	1770 V	240 V
f_0	Network voltage frequency	50 Hz	50 Hz
k	Onboard transformer ratio	15.54	12
L_S^*	Network equivalent inductance	25 mH for LFO and 12.5 mH for harmonic instability	30 mH for LFO and 16.7 mH for harmonic instability
R_S^*	Network equivalent resistance	12.6 mΩ for LFO and 6.3 mΩ for harmonic instability	0 Ω
C_S^*	Network equivalent capacitance	2.8 μF	2.1 μF
$L_{\rm in}$	Leakage inductance of the onboard transformer	6 mH	14 mH
$R_{\rm in}$	Leakage resistance of the onboard transformer	0.01 Ω	0 Ω
R_L	Load resistance	1000 Ω for LFO and 50 Ω for harmonic instability	1000 Ω for LFO and 50 Ω for harmonic instability
C_d	DC-link capacitance	9 mF	4.4 mF
T_d	Time delay	1.2 ms	1.2 ms
f_S	Switching frequency of the 4QC	1250 Hz	1250 Hz
$U_{\rm dc}$	DC voltage of the 4QC	3600 V	40 V
U_{d0}	d channel voltage of the 4QC	2503 V	20 V
U_{q0}	q channel voltage of the 4QC	0 V	0 V
$Kp_{\_\rm VC}$	Proportional gain of the 4QC voltage controller	1	0.1
$Ki_{\_\rm VC}$	Integrator gain of the 4QC voltage controller	0.5	0.025
$Kp_{\_\rm PLL}$	Proportional gain of the 4QC PLL	2	1
$Ki_{\_\rm PLL}$	Integrator gain of the 4QC PLL	60	30
$Kp_{\_\rm CC}$	Proportional gain of the 4QC current controller	0.8	3 for LFO and 7 for harmonic instability
$Ki_{\_\rm CC}$	Integrator gain of the 4QC current controller	2	0.15

VI. CONCLUSION

This paper presented the field measurements for demonstrating the train–network interaction phenomena, including the LFO, harmonic resonance, and harmonic instability in HSR systems. An impedance-based models of multiple trains and traction network interactions system considering the available components and parameters is presented to investigate the formation mechanism and impedance behaviors of the three phenomena. The detailed modeling of the trains and traction network have been represented to construct a unified train–network numerous and experimental system. The low-, medium-, and high-frequency input admittance behavior of the electric train is the primary task as well as the linear traction network to investigate the train–network interactions. The output impedance of the traction network and train are obtained by both theoretical analysis and measurements. The results can be effective for investigating the traction system compatibility for modern electric train system. Finally, the generalized simulation model

and experiment are developed where all the available factors or parameters are included.

APPENDIX A

The rail-to-earth conductance $\mathbf{G}$ is 2 S/km(typical value) and up to 20 S/km. $Z_1 = 6.915 + j160.1$, $Z_2 = Z_3 = 0.268 + j3.94$; the impedance of the AT is $Z_2 = 0.667 + j1.607$.

REFERENCES

[1] E. Mollerstedt and B. Bernhardsson, "Out of control because of harmonics-an analysis of the harmonic response of an inverter locomotive," *IEEE Control Syst.*, vol. 20, no. 4, pp. 70–81, Aug. 2000.

[2] H. Lee, C. Lee, G. Jang, and S. H. Kwon, "Harmonic analysis of the Korean high-speed railway using the eight-port representation model," *IEEE Trans. Power Del.*, vol. 21, no. 2, pp. 979–986, Mar. 2006.

[3] Z. He, H. Hu, Y. Zhang, and S. Gao, "Harmonic resonance assessment to traction power-supply system considering train model in China high-speed railway," *IEEE Trans. Power Del.*, vol. 29, no. 4, pp. 1735–1743, Oct. 2013.

[4] *Power Supply and Rolling Stock - Technical Criteria for the Coordination Between Power Supply and Rolling Stock to Achieve Interoperability*, EN 50388 Standard, 2012.

[5] H. Wang, M. Wu, and J. Sun, "Analysis of low-frequency oscillation in electric railways based on small-signal modeling of vehicle-grid system in dq frame," *IEEE Trans. Power Electron.*, vol. 30, no. 9, pp. 5318–5330, Jan. 2015.

[6] S. Danielsen, M. Molinas, T. Toftevaag, and O. B. Fosso, "Constant power load characteristic's influence on the low-frequency interaction between advanced electrical rail vehicle and railway traction power supply with rotary converters," *Electromotion*, vol. 17, no. 1, p. 61, Jan. 2010.

[7] L. Harnefors, A. Yepes, A. Vidal, and J. Doval-Gandoy, "Passivity-based controller design of grid-connected VSCs for prevention of electrical resonance instability," *IEEE Trans. Ind. Electron.*, vol. 62, no. 2, pp. 702–710, Feb. 2015.

[8] K. Song, M. Wu, V. G. Agelidis, and H. Wang, "Line current harmonics of three-level neutral-point-clamped electric multiple unit rectifiers: analysis, simulation and testing," *IET Power Electron.*, vol. 7, no. 7, pp. 1850–1858, Jul. 2014.

[9] G. W. Chang, H. W. Lin, and S. K. Chen, "Modeling characteristics of harmonic currents generated by high-speed railway traction drive converters," *IEEE Trans. Power Del.*, vol. 19, no. 2, pp. 766–773, Mar. 2004.

[10] X. Wang, F. Blaabjerg, and W. Wu, "Modeling and analysis of harmonic stability in an AC power-electronics-based power system," *IEEE Trans. Power Electron.*, vol. 29, no. 12, pp. 6421–6432, Feb. 2014.

[11] L. Guo, Q. Li, and Y. Xu, "Study on harmonic resonance of traction line in electrified high-speed traction system," in *Proc. Int. Conf. Sustain. Power Gen. Supply*, 2009, pp. 1–4.

[12] H. Hu, M. Zhang, C. Qian, Z. He, and L. Fang, "Research on the harmonic transmission characteristic and the harmonic amplification and suppression in high-speed traction system," in *Proc. Asia-Pac. Power Energy Eng. Conf.*, 2011, pp. 1–4.

[13] M. Brenna, F. Foiadelli, and D. Zaninelli, "Electromagnetic model of high speed railway lines for power quality studies," *IEEE Trans. Power Syst.*, vol. 25, no. 3, pp. 1301–1308, Mar. 2010.

[14] A. Dolara, M. Gualdoni, and S. Leva, "Impact of high-voltage primary supply lines in the 2 × 25 kV-50 Hz railway system on the equivalent impedance at pantograph terminals," *IEEE Trans. Power Del.*, vol. 27, no. 1, pp. 164–175, Oct. 2012.

[15] M. Brenna, A. Capasso, M. C. Falvo, F. Foiadelli, R. Lamedica, and D. Zaninelli, "Investigation of resonance phenomena in high speed railway supply systems: Theoretical and experimental analysis," *Electr. Power Syst. Res.*, vol. 81, no. 10, pp. 1915–1923, Oct. 2011.

[16] M. A. Eitzmann, J. J. Paserba, J. M. Undrill, and C. Amicarella, "Model development and stability assessment of the Amtrak 25 Hz traction system from New York to Washington DC," in *Proc. Railroad Conf.*, Boston, MA, USA, 1997, pp. 21–28.

[17] H. B. P. Schmidt, "Die dezentrale Bahnenergieversorgung von 162/3-Hz Einphasen-wechselstrombahnen über synchron-synchorn-umformer," *Elektr. Bahnen*, vol. 11, no. 89, pp. 179–181, 1991.

[18] S. Danielsen, "Electric traction power system stability: Low-frequency interaction between advanced rail vehicles and a rotary frequency converter," Ph.D. dissertation, Radiat. Lab., Norwegian Univ. Sci. Technol., Trondheim, Norway, 2010.

[19] S. Danielsen and T. Toftevaag, "Experiences with respect to low frequency instability from operation of advanced electrical rail vehicles in a traction power system with rotary converters," in *8th Int. Conf. Modern Electric Traction*, Warsaw, Poland, pp. 51–57, 2007.

[20] D. Frugier and P. Ladoux, "Voltage disturbances on 25 kV-50 Hz railway lines—Modelling method and analysis," in *Proc. Speedam*, 2010, pp. 1080–1085.

[21] B. S. M. Prölss, "Stabiltätskriterien für wechselwirkungen mit umrichteranlagen in bahnsystemen," *Elektr. Bahnen*, vol. 11, no. 104, pp. 542–552, 2006.

[22] M. Debruyne, "Low frequency instability in the Amtrak's 12 kV-25Hz network," in *Proc. Interact. Workshop 2006 Thun*, Switzerland, pp., 2006.

[23] S. Menth and M. Meyer, "Low frequency power oscillations in electric railway systems," *Elektr. Bahnen*, vol. 104, no. 4, pp. 216–221, 2006.

[24] W. Song, S. Jiao, Y. W. Li, and J. Wang, "High-frequency harmonic resonance suppression in high-speed railway through single-phase traction converter with LCL filter," *IEEE Trans. Transp. Electrif.*, vol. 2, no. 3, pp. 347–356, Jun. 2016.

[25] R. Kadhim and D. Kelsey, "25 kV Harmonic resonance modelling on the channel tunnel rail link," in *Proc. Inst. Eng. Technol. Semin. EMC Railw.*, Birmingham, England, Mar. 2006, pp. 137–151.

[26] L. Sainz, M. Caro, and E. Caro, "Analytical study of the series resonance in power systems with the Steinmetz circuit," *IEEE Trans. Power Del.*, vol. 24, no. 4, pp. 2090–2098, Sep. 2009.

[27] J. D. Ainsworth, "Harmonic instability between controlled static convertors and a.c. networks," *Proc. Inst. Elect. Eng.*, vol. 114, no. 7, pp. 949–957, 1967.

[28] L. H. Kocewiak, J. Hjerrild, and C. L. Bak, "Wind turbine converter control interaction with complex wind farm systems," *IET Renew. Power Gener.*, vol. 7, no. 4, pp. 380–389, Jun. 2013.

[29] J. H. R. Enslin and P. J. M. Heskes, "Harmonic interaction between a large number of distributed power inverters and the distribution network," *IEEE Trans. Power Electron.*, vol. 4, no. 6, pp. 1586–1593, Nov. 2004.

[30] J. Rocabert, A. Luna, F. Blaabjerg, and P. RodríGuez, "Control of power converters in AC microgrids," *IEEE Trans. Power Electron.*, vol. 27, no. 11, pp. 4734–4749, May 2012.

[31] A. B. Nassif, J. Yong, and W. Xu, "Measurement-based approach for constructing harmonic models of electronic home appliances," in *Proc. IEE Gener. Transm. Distrib.*, 2010, vol. 4, no. 3, pp. 363–375.

[32] M. Fauri, "Harmonic modelling of non-linear load by means of crossed frequency admittance matrix," *IEEE Trans. Power Syst.*, vol. 12, no. 4, pp. 1632–1638, Nov. 1997.

[33] Y. Sun, G. Zhang, W. Xu, and J. G. Mayordomo, "A harmonically coupled admittance matrix model for AC/DC converters," *IEEE Trans. Power Syst.*, vol. 22, no. 4, pp. 1574–1582, Oct. 2007.

[34] M. Esmaili, H. A. Shayanfar, and A. Jalilian, "Modal analysis of power systems to mitigate harmonic resonance considering load models," *Energy*, vol. 33, no. 9, pp. 1361–1368, Sep. 2008.

[35] K. Song, M. Wu, V. G. Agelidis, and H. Wang, "Line current harmonics of three-level neutral-point-clamped electric multiple unit rectifiers: Analysis, simulation and testing," *IET Power Electron.*, vol. 7, no. 7, pp. 1850–1858, Jul. 2014.

[36] H. Hu, Z. He, X. Li, and K. Wang, "Power-quality impact assessment for high-speed railway associated with high-speed trains using train timetable—Part I: Methodology and modeling," *IEEE Trans. Power Del.*, vol. 2, no. 31, pp. 693–703, Oct. 2015.

[37] S. Danielsen, O. B. Fosso, and M. Molinas *et al.*, "Simplified models of a single-phase power electronic inverter for railway power system stability analysis—Development and evaluation," *Electr. Power Syst. Res.*, vol. 80, no. 2, pp. 204–214, Feb. 2010.

[38] S. Lissandron, L. D. Santa, P. Mattavelli, and B. Wen, "Experimental validation for impedance-based small-signal stability analysis of single-phase interconnected power systems with grid-feeding inverters," *IEEE J. Emerg. Sel. Top. Power Electron.*, vol. 4, no. 1, pp. 103–115, Sep. 2015.

[39] M. Zhao, X. Yuan, J. Hu, and Y. Yan, "Voltage dynamics of current control time-scale in a VSC-connected weak grid," *IEEE Trans. Power Syst.*, vol. 31, no. 4, pp. 2925–2937, Nov. 2016.

[40] L. Harnefors, M. Bongiorno, and S. Lundberg, "Input-admittance calculation and shaping for controlled voltage-source converters," *IEEE Trans. Ind. Electron.*, vol. 54, no. 6, pp. 3323–3334, Nov. 2007.

[41] X. Wang, L. Harnefors, and F. Blaabjerg, "A unified impedance model of grid-connected voltage-source converters," *IEEE Trans. Power Electron.*, vol. 33, no. 2, pp. 1775–1787, Apr. 2017.

[42] Z. He, Z. Zheng, and H. Hu, "Power quality in high-speed railway systems," *Int. J. Rail Transp.*, vol. 4, no. 2, pp. 71–97, Feb. 2016.

[43] Y. Wang, X. Wang, F. Blaabjerg, and Z. Chen, "Harmonic instability assessment using state-space modeling and participation analysis in inverter-fed power systems," *IEEE Trans. Ind. Electron.*, vol. 64, no. 1, pp. 806–816, Jul. 2016.
[44] T. H. Chen and H. Y. Kuo, "Network modelling of traction substation transformers for studying unbalance effects," in *Proc. IEE Gener. Transm. Distrib.*, vol. 142, no. 2, pp. 103–108, Mar. 1995.
[45] R. Cella, G. Giangaspero, A. Mariscotti, and A. Montepagano, "Measurement of AT electric railway system currents at power-supply frequency and validation of a multi-conductor transmission-line model," *IEEE Trans. Power Del.*, vol. 21, no. 3, pp. 1721–1726, Jun. 2006.
[46] M. Wu, "Physical interpretation of impedance formulas for conductors enclosed in a cylindrical tunnel," *IEEE Trans. Power Del.*, vol. 26, no. 3, pp. 1354–1360, Apr. 2011.
[47] M. Wu and Y. Fang, "Numerical calculations of internal impedance of solid and tubular cylindrical conductors under large parameters," in *Proc. IEE Gener. Transm. Distrib.*, 2004, vol. 151, no. 1, pp. 67–72.
[48] M. Brenna, F. Foiadelli, and D. Zaninelli, "Electromagnetic model of high speed railway lines for power quality studies," *IEEE Trans. Power Syst.*, vol. 25, no. 3, pp. 1301–1308, Aug. 2010.

Haitao Hu (S'13–M'14) received the B.S. degree from Zhengzhou University, Zhengzhou, China, in 2010, and the Ph.D. degree from Southwest Jiaotong University, Chengdu, China, in 2014, all in electrical engineering.

From 2013 to 2014, he was a Visiting Doctoral Scholar at the University of Alberta, Edmonton, AB, Canada. He is currently an Associate Professor with the School of Electrical Engineering, Southwest Jiaotong University. His current research interests include power quality and stability of electric traction systems.

Haidong Tao (S'17) received the B.S. degree in electrical engineering in 2015 from Southwest Jiaotong University, Chengdu, China, where he is currently working toward the Ph.D. degree in electrical engineering.

His current research interests include modeling and control of high-speed trains and grid-connected converters, harmonics analysis and control, and stability of power-electronic-based power systems.

Frede Blaabjerg (S'86–M'88–SM'97–F'03) received the Ph.D. degree in electrical engineering from Aalborg University, Aalborg, Denmark, in 1995.

From 1987 to 1988, he was with ABB-Scandia, Randers, Denmark. He became an Assistant Professor in 1992, an Associate Professor in 1996, and a Full Professor of Power Electronics and Drives in 1998. In 2017, he became a Villum Investigator at Aalborg University. His current research interests include power electronics and its applications, such as in wind turbines, PV systems, reliability, harmonics, and adjustable speed drives. He has authored or coauthored more than 500 journal papers in the fields of power electronics and its applications. He is the coauthor of two monographs and editor of six books in power electronics and its applications.

Dr. Blaabjerg was the recipient of 24 IEEE Prize Paper Awards, the IEEE PELS Distinguished Service Award in 2009, the EPE-PEMC Council Award in 2010, the IEEE William E. Newell Power Electronics Award 2014, and the Villum Kann Rasmussen Research Award 2014. He was the Editor-in-Chief of the IEEE TRANSACTIONS ON POWER ELECTRONICS from 2006 to 2012. He has been a Distinguished Lecturer for the IEEE Power Electronics Society from 2005 to 2007 and for the IEEE Industry Applications Society from 2010 to 2011 as well as 2017 to 2018. He was nominated in 2014, 2015, 2016 and 2017 by Thomson Reuters to be one of the 250 most cited researchers in engineering in the world. In 2017, he became Honoris Causa at the University Politehnica Timisoara (UPT), Romania.

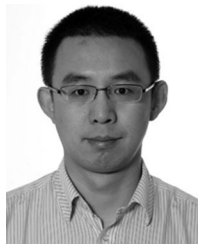

Xiongfei Wang (S'10–M'13–SM'17) received the B.S. degree in electrical engineering from Yanshan University, Qinhuangdao, China, in 2006, the M.S. degree in electrical engineering from Harbin Institute of Technology, Harbin, China, in 2008, and the Ph.D. degree in energy technology from Aalborg University, Aalborg, Denmark, in 2013.

Since 2009, he has been with Aalborg University, where he is currently an Associate Professor in the Department of Energy Technology. His current research interests include modeling and control of grid-connected converters, harmonics analysis and control, passive and active filters, stability of power-electronic-based power systems.

Dr. Wang is an Associate Editor for the IEEE TRANSACTIONS ON POWER ELECTRONICS, the IEEE TRANSACTIONS ON INDUSTRY APPLICATIONS, and the IEEE JOURNAL OF EMERGING AND SELECTED TOPICS IN POWER ELECTRONICS. He is also the Guest Editor for the Special Issue "Grid-Connected Power Electronics Systems: Stability, Power Quality, and Protection" in the IEEE TRANSACTIONS ON INDUSTRY APPLICATIONS. He was the recipient of the second prize paper award and the outstanding reviewer award of the IEEE TRANSACTIONS ON POWER ELECTRONICS in 2014 and 2017, respectively; the second prize paper award of the IEEE TRANSACTIONS ON INDUSTRY APPLICATIONS in 2017; and the best paper awards at the IEEE PEDG 2016 and the IEEE PES GM 2017.

Zhengyou He (M'10–SM'13) received the B.Sc. degree and the M. Sc. degree in computational mechanics from Chongqing University, Chongqing, China, in 1992 and 1995, respectively, and the Ph.D. degree from the School of Electrical Engineering, Southwest Jiaotong University, Chengdu, China, in 2001.

He is currently a Professor in the School of Electrical Engineering, Southwest Jiaotong University. His current research interests include signal processing and information theory applied to electrical power systems and application of wavelet transforms in power systems.

Shibin Gao received the B.S. degree, the M.S. degree, and the Ph.D. degree in electrical engineering from Southwest Jiaotong University, Chengdu, China, 1986, 1999, and 2006, respectively.

He is currently a Professor in Southwest Jiaotong University. His current research interests include protection and control of electric traction systems.